Nonadiabatic molecular orientation by polarization-gated ultrashort laser pulses

Cheng Chen, Jian Wu,* and Heping Zeng†
State Key Laboratory of Precision Spectroscopy, East China Normal University, Shanghai 200062, China
(Received 26 April 2010; published 13 September 2010)

We show that the nonadiabatic orientation of diatomic polar molecules can be controlled by polarization-gated ultrashort laser pulses. By finely adjusting the time interval between two circularly polarized pulses of different wavelengths but the same helicity, the orientation direction of the molecules can be twirled. A cloverlike potential is created by using two circularly polarized laser pulses of different wavelengths and opposite helicity, leading to multidirectional molecular orientation along the potential wells, which can be well revealed by a high-order statistics metric of $\langle\langle\cos^3\theta_d\rangle\rangle$.

DOI: 10.1103/PhysRevA.82.033409 PACS number(s): 37.10.Vz, 33.80.−b, 33.15.Bh, 42.50.Wk

I. INTRODUCTION

The study of nonadiabatic (field-free) alignment and orientation of gaseous molecules has attracted much attention for its extensive applications in molecular orbital reconstruction [1], high-harmonic generation [2], chemical reaction control [3], molecular nanomaterial design [4], and ultrashort laser pulse propagation [5]. The field-free alignment of molecules can be achieved through impulsive excitation by ultrashort laser pulses [6,7], while the field-free molecular orientation with distinguishable head versus tail orders can be achieved by using half-cycle terahertz pulses [8–10], a weak electrostatic field combined with intense laser pulses [11], or dual-color laser pulses [12–15]. As the laser-induced molecular alignment and orientation closely depend on the field polarization, the alignment and orientation direction can be readily controlled by varying the polarization of the applied pulses. For instance, linearly polarized laser pulses can align and can orient molecules parallel or perpendicular to the field polarization, and elliptically polarized pulses can create three-dimensional molecular alignment and orientation [16,17]. It is well known that an extremely short linearly polarized pulse can be gated between elliptically polarized pulses by setting a certain time interval between two circularly polarized ultrashort pulses of opposite helicity, which was successfully applied for single attosecond pulse generation [18,19]. Such a polarization gating technique is promising for molecular orientation control.

In this paper, we show that the direction of the molecular orientation can be controlled by finely adjusting the time interval between two circularly polarized ultrashort pulses of different wavelengths but the same helicity. A cloverlike interaction potential can be created by using two circularly polarized ultrashort pulses of different wavelengths and opposite helicity, which supports simultaneous multidirectional field-free molecular orientation control along the minimums of the interaction potential.

II. RESULTS AND DISCUSSIONS

A. Effective Hamiltonian

The polarization-gated laser field created by two circularly polarized laser pulses can be expressed as

$$\begin{aligned}\vec{E}(t) &= E_x(t)\,\hat{e}_x + E_y(t)\,\hat{e}_y \\ &= E_0[g(t+T_d/2)\sin\omega_1(t+T_d/2) \\ &\quad \pm g(t-T_d/2)\sin\omega_2(t-T_d/2)]\hat{e}_x \\ &\quad + E_0[g(t+T_d/2)\cos\omega_1(t+T_d/2) \\ &\quad + g(t-T_d/2)\cos\omega_2(t-T_d/2)]\hat{e}_y, \end{aligned} \tag{1}$$

where $g(t)=\exp(-t^2/\tau_0^2)$, τ_0, E_0, and $\omega_{1(2)}$ are the envelope, temporal duration, amplitude, and carrier frequencies of the circularly polarized laser pulses. T_d is the time interval between the two pulses, and $\hat{e}_x$ and $\hat{e}_y$ are the unit vectors along the x and y axes. The sign $\pm$ accounts for the polarizations of the pulses with the same helicity or opposite helicity, respectively.

The effective Hamiltonian for the interaction of the polarization-gated laser field with a linear molecule can be expressed as

$$\begin{aligned} H(t) &= B_0 J_0(J_0+1) - \tfrac{1}{2}\alpha_\perp\left(E_x^2+E_y^2\right) \\ &\quad - \tfrac{1}{2}\Delta\alpha\left(E_x^2\sin^2\theta\cos^2\varphi + 2E_xE_y\sin^2\theta\cos\varphi\sin\varphi\right. \\ &\quad \left. + E_y^2\sin^2\theta\sin^2\varphi\right) - \tfrac{1}{6}(\beta_{||}-3\beta_\perp)\left(E_x^3\sin^3\theta\cos^3\varphi\right. \\ &\quad + 3E_x^2E_y\sin^3\theta\cos^2\varphi\sin\varphi \\ &\quad \left. + 3E_xE_y^2\sin^3\theta\cos\varphi\sin^2\varphi + E_y^3\sin^3\theta\sin^3\varphi\right) \\ &\quad - \tfrac{1}{2}\beta_\perp\left(E_x^2+E_y^2\right)(E_x\sin\theta\cos\varphi + E_y\sin\theta\sin\varphi), \end{aligned} \tag{2}$$

where B_0, J_0, θ, and φ are the molecular rotational constant, the molecular rotational momentum, the angle between the molecular axis and the z axis, and the angle between the projection of the molecular axis on the x-y plane and the x axis, respectively. $\alpha_{||}$, $\alpha_\perp$, $\beta_{||}$, and $\beta_\perp$ are the polarizability and hyperpolarizability components parallel and perpendicular to the molecular axis, and $\Delta\alpha=\alpha_{||}-\alpha_\perp$ is the polarizability difference. The first term on the right side of Eq. (2) is the field-free Hamiltonian, and the terms related to the molecular polarizability and hyperpolarizability contribute

*jwu@phy.ecnu.edu.cn
†hpzeng@phy.ecnu.edu.cn

for the molecular alignment and orientation, respectively. For molecular CO, the molecular parameters are $B_0 = 3.83 \times 10^{-23}$ J, $\Delta\alpha = 5.83 \times 10^{-41}$ C^2 m^2 J^{-1}, $\beta_{||} = 1.02 \times 10^{-51}$ C^3 m^3 J^{-2}, and $\beta_\perp = 1.85 \times 10^{-52}$ C^3 m^3 J^{-2} [20], respectively.

B. FW and SH with same helicity

As compared with molecular alignment, molecular orientation requires an asymmetric laser field to change the molecular wave-function parity. Here, two circularly polarized fundamental-wave (FW) and second-harmonic (SH) pulses with carrier frequencies of $\omega_2 = 2\omega_1 = 2\omega$ are considered for the polarization-gated laser field. For FW and SH circularly polarized pulses with the same helicity, the cycle-averaged effective Hamiltonian reduces to

$$\begin{aligned} H_{\text{eff}}(t) = {} & B_0 J_0(J_0+1) - \tfrac{1}{4}\Delta\alpha E_0^2[g^2(t+T_d/2) \\ & + g^2(t-T_d/2)]\sin^2\theta - \tfrac{1}{8}(\beta_{||} - 3\beta_\perp) \\ & \times E_0^3 g^2(t+T_d/2)g(t-T_d/2)\sin^3\theta\sin(\varphi+2\omega T_d) \\ & - \tfrac{1}{2}\beta_\perp E_0^3 g^2(t+T_d/2)g(t-T_d/2) \\ & \times \sin\theta\sin(\varphi+2\omega T_d). \end{aligned} \tag{3}$$

It indicates that the minimum of the interaction potential with hyperpolarizability for molecular orientation (the third and fourth terms on the right side of the effective Hamiltonian) locates at $\theta_1 = \pi/2$ and $\varphi_1 = \pi/2 - 2\omega T_d$, which closely depends on the time interval T_d between the FW and SH pulses with the same helicity. This provides us with an effective approach to control the molecular orientation direction along the minimums of the potential well by finely adjusting the time interval T_d.

We calculate the molecular orientation by numerically solving the time-dependent Schrödinger equation $i\hbar\partial|\psi\rangle/\partial t = H_{\text{eff}}(t)|\psi\rangle$ for the evolution of the rotational state $|\psi\rangle = \sum_{JM} C_{JM}|JM\rangle$. The molecular orientation metrics are calculated for each initial rotational state $|J_0M_0\rangle$, and are then assembled by considering their temperature-dependent Boltzmann distribution and eventually lead to the observable molecular orientation evolution [21]. Figure 1(a) shows the simulated field-free orientation of molecular CO for an initial temperature of 30 K. Here, the peak intensity and temporal duration of each circularly polarized laser pulse are set to be 3.0×10^{13} W/cm^2 and 50 fs (full width at half maximum), respectively. The central wavelengths of the FW and SH pulses are set to be 800 and 400 nm, respectively. The molecular orientation with respect to the detection direction $\hat{e}_d$ is denoted by $\langle\langle\cos\theta_d\rangle\rangle$ with θ_d being the angle between the directions $\hat{e}_{\text{mol}}$ and $\hat{e}_d$, where $\hat{e}_{\text{mol}} = (\sin\theta\cos\varphi, \sin\theta\sin\varphi, \cos\theta)$ is the unit vector of the molecular axis and $\hat{e}_d = \hat{e}_x, \hat{e}_y, \hat{e}_{\text{well}_{||}}, \hat{e}_{\text{well}_\perp}$. The unit vectors $\hat{e}_{\text{well}_{||}} = (\cos\varphi_1, \sin\varphi_1, 0)$ and $\hat{e}_{\text{well}_\perp} = (\cos\varphi_2, \sin\varphi_2, 0)$ describe the azimuth of the potential well and the direction perpendicular to the potential

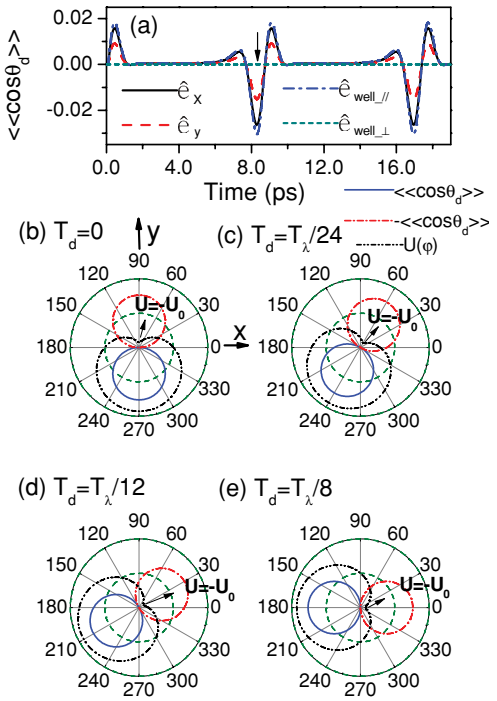

FIG. 1. (Color online) (a) Temporal evolution of molecular orientation observed from various detection directions for $T_d = T_\lambda/12$. The simulated field-free molecular orientation distribution (blue solid and red dash-dotted curves) around the full revival time [$t = 8.30$ ps, as marked with an arrow in (a)] in the x-y plane for different time intervals T_d (from 0 to $T_\lambda/8$) is shown in (b)–(e), which is rotated by closely following the rotation of the potential well (black dash-dot-dotted curves). The blue solid and red dash-dotted curves stand for the positive and negative molecular orientation, respectively, and the olive dashed circles represent the potential $U = 0$.

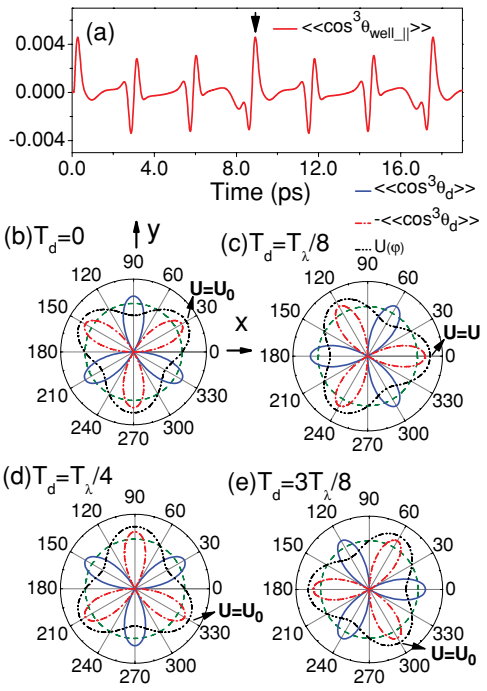

FIG. 2. (Color online) (a) Temporal evolution of molecular orientation observed from the potential well. Cloverlike potential wells (black dash-dot-dotted curves) created by the dual-color circularly polarized pulses of opposite helicity, and the corresponding multidirectional molecular orientation (blue solid and red dash-dotted curves) characterized by $\langle\langle\cos^3\theta_d\rangle\rangle$ around the full revival time ($t = 8.92$ ps) for different time intervals are shown in (b)–(e).

well, respectively, where $\theta_2 = \pi/2$ and $\varphi_2 = -2\omega T_d$. For $T_d = T_\lambda/12$, the potential well along $\varphi_1 = \pi/6$ has a larger projection on the x axis than that on the y axis, which accounts for a larger molecular orientation degree of $\langle\langle\cos\theta_x\rangle\rangle$ than $\langle\langle\cos\theta_y\rangle\rangle$ as shown in Fig. 1(a). Meanwhile, the molecular orientation is detected with the maximum degree from the direction parallel to the potential well with $\langle\langle\cos\theta_{\text{well}_\parallel}\rangle\rangle$ but with zero from the perpendicular direction with $\langle\langle\cos\theta_{\text{well}_\perp}\rangle\rangle$. As shown in Figs. 1(b)–1(e) (black dash-dot-dotted curves), by adjusting the time interval T_d from 0 to $T_\lambda/8$, the direction of the potential well ($U = -U_0$) rotates from the y axis to the x axis. Correspondingly, as shown in Figs. 1(b)–1(e), the direction of the field-free molecular orientation around the full revival time ($t = 8.30$ ps) is controllably rotated by closely following the rotation of the hyperpolarizability-related interaction potential well. Here, the blue solid and red dashed-dotted curves stand for the positive and negative molecular orientations with more oxygen or carbon atoms orientated along the unit vectors, respectively. Therefore, by finely adjusting the time interval between two circularly polarized pulses of the same helicity, the direction of the molecular orientation can be controllably rotated in the polarization plane. For a larger time interval of several optical cycles, the molecular orientation direction control is still valid, but the molecular orientation degree is decreased for the reduced effective temporal duration of the dual-color laser field.

C. FW and SH with opposite helicity

Beyond the rotation of the molecular orientation direction by using FW and SH pulses of the same helicity, a cloverlike multidirection molecular orientation can be achieved by using circularly polarized FW and SH pulses of opposite helicity. For this case, the cycle-averaged Hamiltonian takes the form

$$H_{\text{eff}}(t) = B_0 J_0(J_0+1) - \tfrac{1}{4}\Delta\alpha E_0^2[g^2(t+T_d/2) + g^2(t-T_d/2)]\sin^2\theta + \tfrac{1}{8}(\beta_{\parallel}-3\beta_{\perp})E_0^3 g^2(t+T_d/2) \times g(t-T_d/2)\sin^3\theta\sin(3\varphi+2\omega T_d). \quad (4)$$

Interestingly, as we can see from the third term on the right side of Eq. (4), there exist three minimums for the hyperpolarizability-related interaction potential in the polarization plane, which locate at $\varphi = \pi/2 - 2\omega T_d/3$, $-\pi/6 - 2\omega T_d/3$, and $7\pi/6 - 2\omega T_d$, respectively. Since the molecules tend to orientate along the minimums of the potential well, this cloverlike potential structure can be used for multidirectional molecular orientation. However, when the conventional molecular orientation metric $\langle\langle\cos\theta_d\rangle\rangle$ is used for the measurement, zero net molecular orientation measurement will result for this symmetrical cloverlike interaction potential. In order to show this highly symmetrical cloverlike multidirectional molecular orientation, we use an extended metric of $\langle\langle\cos^3\theta_d\rangle\rangle$ to characterize the actually existing cloverlike molecular orientation. A similar description of the higher-order orientation metric based on the spherical tensor can be found in Ref. [22]. Figure 2(a) shows the temporal evolution of molecular orientation metric $\langle\langle\cos^3\theta_d\rangle\rangle$. The black dash-dot-dotted curves in Figs. 2(b)–2(e) show the cloverlike interaction potential created by the dual-color circularly polarized pulses of opposite helicity, and the corresponding multidirection molecular orientation characterized by $\langle\langle\cos^3\theta_d\rangle\rangle$ around the full revival time ($t = 8.92$ ps) is presented with the blue solid and red dash-dotted curves. Similarly, the cloverlike interaction potential wells can be rotated as the time interval T_d ($\Delta\varphi = 2\omega\Delta T_d/3$) increases,

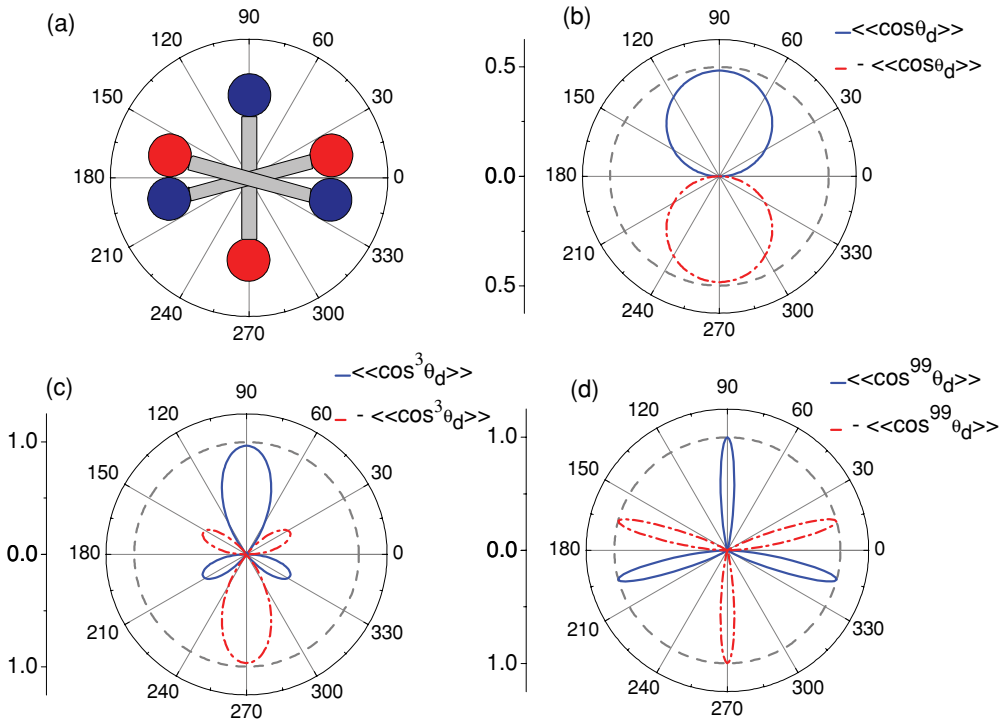

FIG. 3. (Color online) The characterizations of (a) three diatomic polar molecules orientated at $\theta = 90^\circ$, 195°, and 345° by the orientation metrics of (b) $\langle\langle\cos\theta_d\rangle\rangle$, (c) $\langle\langle\cos^3\theta_d\rangle\rangle$, and (d) $\langle\langle\cos^{99}\theta_d\rangle\rangle$, respectively.

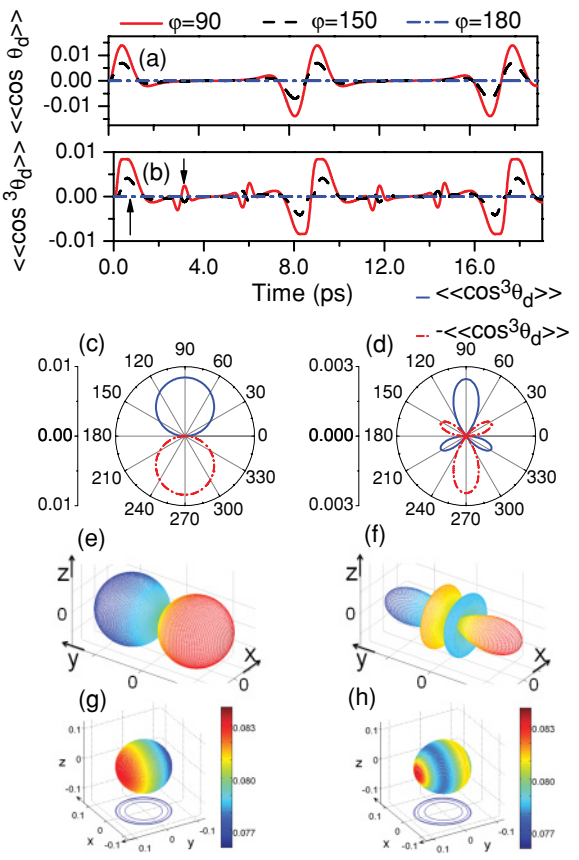

FIG. 4. (Color online) Temporal evolutions of the molecular orientation metrics of (a) $\langle\langle\cos\theta_d\rangle\rangle$ and (b) $\langle\langle\cos^3\theta_d\rangle\rangle$ for an interaction potential of $-U_0\sin^3\theta\sin^3\varphi$ by detecting from various directions in the polarization plane. The distribution of $\langle\langle\cos^3\theta_d\rangle\rangle$ in the polarization plane (c),(d), the molecular orientation distribution (e),(f), and the molecular rotational wave-function probability distribution (g),(h) for evolution times at $t = 0.6$ ps (left column) and 3.14 ps (right column) [as marked with arrows in (b)] are shown in (c)–(h), respectively.

leading to the rotation of the multidirectional molecular orientation as shown in Figs. 2(b)–2(e).

D. The high-order orientation tensor

The fact that the high-order symmetrical multidirectional molecular orientation can be characterized by $\langle\langle\cos^3\theta_d\rangle\rangle$ rather than the conventional $\langle\langle\cos\theta_d\rangle\rangle$ can be understood by following the instant example of three diatomic polar molecules as shown in Fig. 3(a). Figure 3(b) shows the conventional metric $\langle\langle\cos\theta_d\rangle\rangle$ of the molecules with $\langle\langle\cos\theta_d\rangle\rangle = \sum A_i\cos(\theta_d-\theta_i) = A_m\cos(\theta_d-\theta_m)$, where A_i is the probability of molecules oriented at $\theta=\theta_i$. Since $\langle\langle\cos\theta_d\rangle\rangle$ has only one maximum, it shows only one direction of orientation as plotted in Fig. 3(b). The ideal parameter to characterize the distribution of the molecular orientation should have the form of a δ function with its weight to be 1 only in the direction of measurement and 0 in other directions, which can be expressed as $\langle\langle\cos^n\theta_d\rangle\rangle$ with n approaching infinity. The bigger n is, the more rapidly the value of $\langle\langle\cos^n\theta_d\rangle\rangle$ descends in the vicinity of $\theta\sim\theta_d$, and therefore the closer the measurement is with respect to the real distribution of the molecular orientation. As plotted in Fig. 3(d), the maximums of $\langle\langle\cos^{99}\theta_d\rangle\rangle$ are located at $\theta_d = 90°, 195°$, and 345° with equal values, corresponding to the actual molecular orientation distribution.

Furthermore, as shown in Figs. 4(a) and 4(b), for another interaction potential of $-U_0^3\sin^3\theta\sin^3\varphi$ with $U_0 = 10B_0g^3(t)$, the contrast of the temporal evolution between $\langle\langle\cos\theta_d\rangle\rangle$ and $\langle\langle\cos^3\theta_d\rangle\rangle$ is observable. The metric $\langle\langle\cos^3\theta_d\rangle\rangle$ varies at about one-third and two-thirds revivals, while $\langle\langle\cos\theta_d\rangle\rangle$ remains zero. Further exploration of the distribution of $\langle\langle\cos^3\theta_d\rangle\rangle$ shows that molecules are oriented in one direction at $t = 0.6$ ps [see Fig. 4(c)], and multidirectionally oriented at $t = 3.14$ ps [see Fig. 4(d)], which are similar to the real molecular orientation distribution as shown in Figs. 4(e) and 4(f). Figures 4(g) and 4(h) show the asymmetric rotational wave-function probability distribution of the molecules, and the orientation distribution is acquired from the difference between the distributions of the two different atoms.

III. CONCLUSION

To summarize, we have shown that the field-free molecular orientation could be controlled by using polarization-gated laser fields of different wavelengths. By finely adjusting the time interval between the circularly polarized pulses, the created interaction potential well and consequently the molecular orientation direction can be continuously rotated in the polarization plane. Spatially symmetric multidirectional molecular orientation is predicted by using a polarization-gated laser field consisting of FW and SH pulses of opposite helicity, and is characterized by $\langle\langle\cos^3\theta_d\rangle\rangle$, which is helpful to illustrate the fine structure of the molecular multidirectional orientation.

ACKNOWLEDGMENTS

This work was partly funded by the National Natural Science Fund (Grants No. 10525416 and No. 10804032), the National Key Project for Basic Research (Project No. 2006CB806005), and Projects from the Shanghai Science and Technology Commission (Projects No. 08ZR1407100 and No. 09QA1402000).

[1] J. Itatani, J. Levesque, D. Zeidler, H. Niikura, H. Pepin, J. C. Kieffer, P. B. Corkum, and D. M. Villeneuve, Nature (London) **432**, 867 (2004).

[2] R. Velotta, N. Hay, M. B. Mason, M. Castillejo, and J. P. Marangos, Phys. Rev. Lett. **87**, 183901 (2001).

[3] J. J. Larsen, I. Wendt-Larsen, and H. Stapelfeldt, Phys. Rev. Lett. **83**, 1123 (1999).

[4] B. K. Dey, M. Shapiro, and P. Brumer, Phys. Rev. Lett. **85**, 3125 (2000).

[5] J. Wu *et al.*, Opt. Lett. **33**, 2593 (2008); J. Wu, H. Cai, Y. Peng, and H. Zeng, Phys. Rev. A **79**, 041404(R) (2009); H. Cai, J. Wu,

P. Lu, X. Bai, L. Ding, and H. Zeng, *ibid.* **80**, 051802(R) (2009); J. Wu *et al.*, Opt. Lett. **34**, 3211 (2009); Appl. Phys. Lett. **95**, 221502 (2009).

[6] B. Friedrich and D. Herschbach, Phys. Rev. Lett. **74**, 4623 (1995).

[7] H. Sakai, C. P. Safvan, J. J. Larsen, K. M. Hilligsøe, K. Hald, and H. Stapelfeldt, J. Chem. Phys. **110**, 10235 (1999).

[8] M. Machholm and N. E. Henriksen, Phys. Rev. Lett. **87**, 193001 (2001).

[9] C. M. Dion, A. Keller, and O. Atabek, Eur. Phys. J. D **14**, 249 (2001).

[10] A. Matos-Abiague and J. Berakdar, Phys. Rev. A **68**, 063411 (2003).

[11] O. Ghafur, A. Rouzée, A. Gijsbertsen, W. K. Siu, S. Stolte, and M. J. J. Vrakking, Nat. Phys. **5**, 289 (2009).

[12] M. J. J. Vrakking and S. Stolte, Chem. Phys. Lett. **271**, 209 (1997).

[13] R. Tehini and D. Sugny, Phys. Rev. A **77**, 023407 (2008).

[14] S. De *et al.*, Phys. Rev. Lett. **103**, 153002 (2009).

[15] J. Wu and H. Zeng, Phys. Rev. A **81**, 053401 (2010).

[16] J. J. Larsen, K. Hald, N. Bjerre, H. Stapelfeldt, and T. Seideman, Phys. Rev. Lett. **85**, 2470 (2000).

[17] H. Tanji, S. Minemoto, and H. Sakai, Phys. Rev. A **72**, 063401 (2005).

[18] P. B. Corkum, N. H. Burnett, and M. Y. Ivanov, Opt. Lett. **19**, 1870 (1994).

[19] G. Sansone *et al.*, Science **314**, 443 (2006).

[20] K. A. Peterson and T. H. Dunning Jr., J. Mol. Struct. (Theochem) **400**, 93 (1997); M. Pecul, Chem. Phys. Lett. **404**, 217 (2005).

[21] J. Wu, H. Cai, A. Couairon, and H. Zeng, Phys. Rev. A **79**, 063812 (2009).

[22] R. N. Zare, *Angular Momentum: Understanding Spatial Aspects in Chemistry and Physics* (Wiley Interscience, New York, 1988).